SUPERSONIC TURBULENT CHANNEL FLOW OVER COMPLEX WALL IMPEDANCE

Yongkai Chen
School of Mechanical Engineering
Purdue University
West Lafayette, IN 47906, USA
chen1305@purdue.edu

Carlo Scalo
School of Mechanical Engineering
Purdue University
West Lafayette, IN 47906, USA
scalo@purdue.edu

ABSTRACT

The study focuses on flow instabilities in supersonic channel flows over assigned wall impedance. Such investigation is carried out via the Time-Domain Impedance Boundary Condition (TDIBC) technique enabling the exact imposition of the wall acoustic response in high-fidelity simulations. This type of boundary condition is applied to bottom wall of compressible turbulent channel flows with two bulk Mach numbers: $M_b = 1.50, 3.50$. Bulk Reynolds number Re_b are selected to ensure similar viscous Reynolds number Re^*_τ that leads to resemblance of near wall turbulence structures at different Mach numbers. A mass-spring-damper impedance model is adopted for TDIBC, with the resonating frequency f_{res} tuned to large eddy turnover frequency. For each Mach number, simulations are performed with various wall acoustic resistance: $R = 0.10, 0.50, 1.00, \infty$. The finite wall impedance results in non-zero wall normal velocity fluctuations. For the same Mach number, wall with lower acoustic resistance R exhibit stronger reaction to the mean flow, reflected by a larger root-mean-square wall normal velocity. For values of R below (including) 0.50, a drastically change in the near wall turbulence structures is observed: the typical near wall streamwise streaks are replaced with spanwise roller, exhibiting the Kelvin-Helmholtz type of instability. With sufficiently high permeability, rollers start to have a strong interaction with the overlying mean flow.

INTRODUCTION

The application of porous walls as acoustic liner has gained its popularity in the past few decades, mainly used as an efficient way for noise reduction in aero engines. When performing numerical simulations including the porous wall, it is not easy to include the detailed geometry directly in the computational domain. An alternative way is to define a proper wall boundary condition that can characterize the wall acoustic property. Such property is usually defined through a complex quantity called acoustic impedance $Z(\omega)$, written as (Kinsler *et al.*, 1999)

$$Z(\omega) = \hat{p}/\hat{v}_n \tag{1}$$

where $\hat{p}$ and $\hat{v}_n$ are the Fourier transform of surface pressure and normal velocity signals, ω is the angular frequency. As one can notice, equation (1) is defined in the Fourier domain. Its time correspondence will be needed if the simulation is performed in time domain, which is usually the case in computational fluid dynamics (CFD) or computational aeroacoustics (CAA) . As a result, a time-domain impedance boundary condition (TDIBC) is of great interest. Efforts have been made to tackle this type of boundary condition since last century. The very first contribution can date back to the work by Ingard (1959), who derived the proper boundary conditions for invicid flow. Later, Myers (1980) extended the result to viscous flow. The combined result is usually referred to as Ingard-Myers condition in the community. A well-known issue of TDIBC is its well-posedness, which is in general related to the form of impedance being used. Tam & Auriault (1996) successfully implemented a three-parameter impedance model with linearized Euler's equations. A set of time domain PDEs can be derived directly from the impedance boundary condition in Fourier domain. This type of TDIBC will be well-posed provided the imaginary part of the impedance has the correct sign. Later, Fung & Ju (2001) constructed the TDIBC based on residue theorem. In this method, the convolution integral deducted from (1) is evaluated numerically through quadrature rule, provided the poles and residues of the wall reflection coefficient. However, this formulation is limited to second order accuracy in time. Dragna *et al.* (2015) improved the accuracy based on Auxiliary Differential Equations (ADE) method. By approximating the impedance with rational function in Fourier domain, the convolution integral can be converted to two auxiliary variable governing by a set of first order PDEs and can be advanced in time with arbitrary order of accuracy. As will be shown later, work presented in this paper uses a slightly variant of this method. A thorough research on the well-posedness of TDIBC gas been done by Rienstra (2006), who derived the mathematical and physical constraints on the impedance model to ensure the validity of TDIBC. Readers are suggested to refer to this paper for interest.

All of the work mentioned above are carried out either for the pure acoustic field, or under the framework of low speed inviscid fluid. Applications of TDIBC in viscous flow, especially wall bounded turbulent flow, have also been investigated. Jiménez *et al.* (2001) performed an Direct Numerical Simulation (DNS) of incompressible plane turbulent channel flow over porous wall, in which the impedance is purely real. It was found that the near wall structure has been significantly altered, reflected by enhancement in near wall spanwise-wise vorticity intensity. Locally blowing and suction regions have been identified, which on average increase the mean wall shear stress. Similar effects are reported by Scalo *et al.* (2015), who conducted a series of numerical experiments of compressible turbulent channel flow over complex wall impedance with isothermal wall condition, spanning a flow regime from nearly incompressible ($M_b = 0.05$) to low subsonic ($M_b = 0.5$). Spanwise rollers, exhibiting Kelvin-Helmholtz type behavior, are found to replace the typical stream-wise streaks. Theses structures are confined in a so-called resonating buffer layer and change only the near wall turbulent activities. The current work is an attempt to investigate the applications of TDIBC in supersonic turbulent flows, extending previous work by Scalo *et al.* (2015).

PROBLEM FORMULATION

In this work, Large Eddy Simulations (LES) of compressible turbulent channel flows over complex wall impedance are investigated. The flow setup is shown in figure 1, with direction $(x,y,z) = (x_1,x_2,x_3)$ representing the streamwise, wall-normal and spanwise drections, respectively. The simulations are performed by solving full set of Favre-filtered compressible Navier-Stokes equations. The eddy viscosity model by Vreman (2004) is used for turbulence closure. Periodic boundary condition is used for streamwise and spanwise directions. Isothermal conditions are applied at both walls. The top wall is kept impermeable and TDIBC is applied at bottom wall for finite impedance. No-slip conditions are used for streamwise and spanwise velocities on both walls. Let δ, a_w and T_w be the channel half-width, wall speed of sound and wall temperature. Also, define bulk density ρ_b as $\rho_b = <\rho>_V$, where the bracket $<\cdot>$ represents the volume average over the computational domain. From here on, all quantities will be presented in non-dimensional form based on these four variables unless otherwise stated.

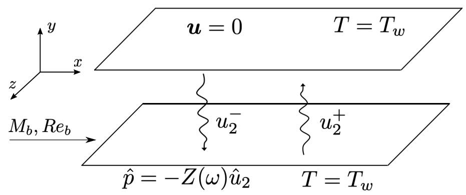

Figure 1. Flow setup for turbulent channel flow over permeable walls. Note that only the bottom wall is set to be permeable, the streamwise and spanwise velocity components at bottom wall are set to be zero.

TDIBC

In this subsection, the formulation of the time-domain impedance boundary condition is introduced. For all work presented here, the Auxiliary Differential Equation (ADE) method (Dragna *et al.*, 2015; Troian *et al.*, 2017) is used for TDIBC. The method is based on what is usually referred to as recursive convolution method developed by Fung & Ju (2004) (see also Fung *et al.* (2000) and Fung & Ju (2001) for more details). This type of method utilizes the residue theorem to evaluate the convolution integral that appears due to the Fourier domain multiplication in (1). Method by Fung & Ju (2004) uses the quadrature rule to evaluate the integral and is limited to second order, while the ADE method relies on an additional set of differential equations of auxiliary variables that can be advanced together with the flow variables and thus can achieve arbitrary order in time. To apply the method, it is more convenient to use the concept of wall softness $\widehat{\widetilde{W}}(\omega) = 2/[1+Z(\omega)]$ to relate the domain-leaving wave v_n^{in} and domain entering wave v_n^{out} via

$$v_n^{\text{in}}(t) = -v_n^{\text{out}}(t) + \int_{-\infty}^{\infty} \widetilde{W}(\tau) v_n^{\text{out}}(t-\tau)d\tau \qquad (2)$$

Care must be taken when evaluating the convolution integral to avoid numerical instabilities, since there are several constraints on TDIBC imposed by physical validity. These constraints will limit the choice of parameters for a given type of impedance model $Z(\omega)$. As clearly stated by Rienstra (2006) and summarized by Douasbin *et al.* (2018)

1. Passive wall assumption. In the scope of this paper, the wall does not produce energy on its own. Thus the acoustic intensity into the wall must always be positive. This requires $\Re(Z(\omega)) \geq 0$.
2. Reality of the signal. Since the pressure and wall normal velocity signals are pure real, the time-domain correspondence $z(t)$ of impedance $Z(\omega)$ must be real, which needs $\widehat{Z}(\omega) = \widehat{Z}^*(-\omega)$
3. Causality. A physical process should not depend on any information from the future.

The three-parameter impedance model (Tam & Auriault, 1996) satisfying all above constraints is used for simulations presented.

$$Z(\omega) = R + j(X_+\omega - X_{-1}\omega^{-1}) \qquad (3)$$

Here R is the acoustic resistance ; X_{+1} is mass-like reactance and X_{-1} the spring-like reactance. The above condition requires $R \geq 0$ for this impedance model. Because of causality, the integration in (2) cannot be performed for $\tau < 0$, ans also zeros of $1+Z(\omega)$ should all in the upper ω-plane. In addition, since time is usually assumed to start from zero, the upper limit of the integration can be replaced by t. Then, equation (2) becomes

$$v_n^{\text{in}}(t) = -v_n^{\text{out}}(t) + \int_{0}^{t} \widetilde{W}(\tau) v_n^{\text{out}}(t-\tau)d\tau \qquad (4)$$

A sum of rational functions is sufficient enough to approximate the wall softness $\widehat{\widetilde{W}}(\omega)$ (see Appendix and Douasbin *et al.* (2018)).Then the integral in equation (4) can be replaced with the summation of n_0 pairs of auxiliary variables $\psi_k^{(1)}$ and $\psi_k^{(2)}$, with $k = 1,2,\cdots n_0$. Each pair of the variables are governed by the following equations

$$\frac{d\psi_k^{(1)}(t)}{dt} = c_{k-1}\psi_k^{(1)}(t) - d_{k-1}\psi_k^{(2)}(t) + v_n^{\text{out}}(t) \qquad (5)$$

$$\frac{d\psi_k^{(2)}(t)}{dt} = c_{k-1}\psi_k^{(2)}(t) + d_{k-1}\psi_k^{(1)}(t) \qquad (6)$$

The domain entering wave is then calculated by

$$v_n^{\text{in}}(t) = -v_n^{\text{out}}(t) + \sum_{k=1}^{n_0} 2[a_k\psi_k^{(1)}(t) - b_k\psi_k^{(2)}] \qquad (7)$$

Please refer to Appendix for detailed derivation.

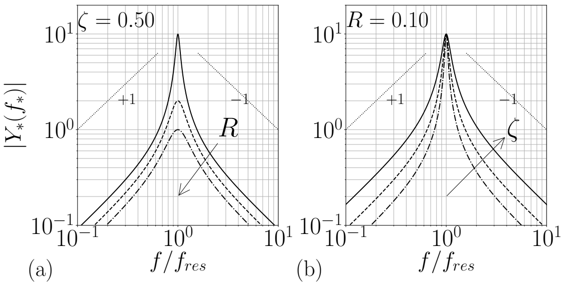

Figure 2. Magnitude of admittance, versus dimensionless frequency for various R (a) and various ζ (b).

Choice of Parameter Space

In current problem, the free parameters includes the flow condition M_b and Re_b, as well as the acoustic parameters in (3), i.e., R, X_{+1} and X_{-1}. A reduction in parameter space is needed to reduce the computation cost. To first ensure the flow speed is in the range of interest, two bulk Mach numbers were chosen: $M_b = 1.50, 3.50$. The bulk Reynolds number Re_b for each Mach number is selected so that the viscous Reynolds number Re^*_τ is kept the same across different Mach numbers. The consideration here is that the TDIBC is reacting to wall pressure fluctuation, which is affected a lot by near wall turbulence structure. To achieve a structure-wise similarity, it is reasonable to choose the bulk Reynolds number so that all cases share similar Re^*_τ. As the result, the flow conditions are chosen as $Re_b = 5000, 10000$ for $M_b = 1.50, 3.50$, respectively, which corresponds to $Re^*_\tau \approx 220$. To choose the acoustic parameters, we first recast the three parameter model into the following form:

$$Z(\omega) = R + i\frac{R+1}{2\zeta}\left[\frac{\omega}{\omega_{\text{res}}} - \frac{\omega_{\text{res}}}{\omega}\right] \quad (8)$$

where $\omega_{\text{res}} = \sqrt{X_{-1}/X_{+1}}$ is the resonating frequency and $\zeta = (1+R)/(2\omega_{\text{res}}X_{+1})$ is the damping ratio. In all simulations presented, the wall impedance is designed to react to large vortical structures, characterized by large-eddy-turnover frequency and thus we simply have $\omega_{\text{res}} = 2\pi M_b$ in dimensionless form. The causality constraints requires requires $0 < \zeta < 1$. To simplify the parameter space of the problem, a value of $\zeta = 0.5$ is chosen for all cases, which is proved to give enough reaction in current simulations. The resistance R has been reported to have strong effect on the flow field Scalo *et al.* (2015). The acoustic admittance $Y(\omega) = \hat{v}_n/\hat{p}$ - the reciprocal of impedance (3) - is directly related to wall permeability, as shown in figure 2. A high value of admittance corresponds to high wall permeability, and is strongly dependent on the resistance R. Values of $R = 0.10, 0.50, 1.00$ are used to study its effect on the flow.

NUMERICAL SETUP

The filtered, Favre average compressible Navier-Stokes equations are solved by using a six order compact finite differencing code developed by Nagarajan *et al.* (2003). Biased compact schemes of third and forth orders are used for spatial discretization of (near) boundary points. Explicit time advancement schemes up to fourth order are available. In current simulation, a fourth order six stages Runge-Kutta scheme (Allampalli *et al.*, 2009) is used for all simulations.

TURBULENT CHANNEL FLOWS

Impermeable Walls

The flow parameters for impermeable wall cases and the grid resolution are listed in Table 1.

Table 1. Grid resolution for baseline cases with impermeable walls. All cases have the same domain size of $L_x \times L_y \times L_z = 12 \times 2 \times 4$.

Case	M_b	Re^*_τ	Δx^+	Δy^+_{min}	Δz^+
$M_{1.5}R_{\text{inf}}$	1.50	220.78	25.25	0.14	11.25
$M_{3.5}R_{\text{inf}}$	3.50	221.79	39.25	0.31	21.85

The normalized mean streamwise velocity is shown in figure 3. Here the transformation law for compressible wall-bounded turbulent flow by Trettel & Larsson (2016) is used to scale the statistics. Note that the distance from the wall y^* is calculated using the semi-local scale (Coleman *et al.*, 1995). For reference, the case with $M_b = 1.50, Re_b = 5000$ by Ulerich *et al.* (2014), and incompressible results by Moser *et al.* (1999) are also plotted. The case $M_{1.5}R_{\text{inf}}$ over predict in the log-law region while $M_{3.5}R_{\text{inf}}$ agrees well with the reference data.

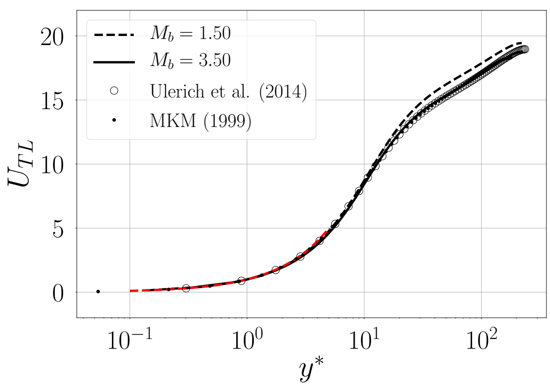

Figure 3. Mean streamwise velocity of turbulent channel flow over impermeable walls.

Figure 4 presents the contour of streamwise Mach number at a wall normal location $y^* \approx 15$. The resemblance of near wall structures between the two Mach numbers can be visually confirmed, which is a result of choosing the same viscous Reynolds number.

Permeable Wall

Parameters of permeable wall simulations are listed in Table 2, together with grid resolution based on length scale calculated with bottom wall properties. It should be pointed out that all permeable wall simulations are performed with a box size $L_x \times L_y \times L_z = 8 \times 2 \times 4$ to reduce the computational cost. The two-point correlation (not shown here) indicates a sufficient box size. Note that the case $M_{3.5}R_{0.1}$ is found to have an extremely strong reaction near the wall,

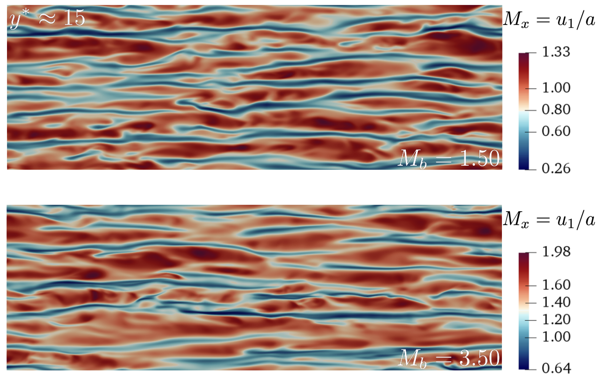

Figure 4. Contour plots of the instantaneous streamwise Mach nubmer at $y^* \approx 15$ for case $M_{1.5}R_{\text{inf}}$ (top) and $M_{3.5}R_{\text{inf}}$ (bottom).

severely limiting the computational speed and data obtained is not enough for analysis yet.

Table 2. Parameters and resolutions of permeable wall cases. For each Mach number, the bulk Reynolds number R_b is the same as the corresponding impermeable wall case.

Case	M_b	R	Δx^+	Δy^+_{min}	Δz^+
$M_{1.5}R_{0.1}$	1.50	0.10	32.58	0.22	16.29
$M_{1.5}R_{0.5}$	1.50	0.50	22.93	0.31	11.46
$M_{1.5}R_{1.0}$	1.50	1.00	21.20	0.30	10.60
$M_{3.5}R_{0.1}$	3.50	0.10	N/A	N/A	N/A
$M_{3.5}R_{0.5}$	3.50	0.50	59.37	0.48	29.68
$M_{3.5}R_{1.0}$	3.50	1.00	48.74	0.39	24.37

Alternation of Near Wall Structures The first observation in flow over the permeable wall is the change in near wall turbulence structures, as shown in figure 5. Here the Q-criterion, wall pressure fluctuation and wall shear stress are shown for $M_b = 3.50$ over an impermeable and permeable wall. Dramatic changes appear in the flow: the typical streamwise and hairpin vortices are replaced by spanwise rollers, residing near the wall. The non-zero wall normal velocity enhances the exchange of the streamwise momentum adjacent to the wall, creating low and high streamwise velocity regions that alternate in the mean flow direction, leading to a same pattern in the wall shear stress. Although the wall shear stress over a permeable wall has locally low-value spots, it is still in general higher than an impermeable wall case on the mean. High permeability causes a tremendous rise in the mean wall shear - up to 156.66% in case $M_{1.5}R_{0.1}$. This enhancement of the wall shear stress is also reported in incompressbile (Jiménez *et al.*, 2001) and subsonic compressible cases (Scalo *et al.*, 2015). It is interesting to notice that the mean shear stress at top wall also experiences changes. At current stage it is hard to tell if this change in upper wall is due to the domain size, or the implementation of TDIBC. It will be left for future investigation. The near wall rollers are found to have a strong interaction with the main flow at sufficiently low resistance. Figure 6 shows the dilatation field of case $M_{3.5}R_{0.5}$ in $x-y$ plane at spanwise station $z = 2.0$, exhibiting a wave-like pattern across the whole channel.

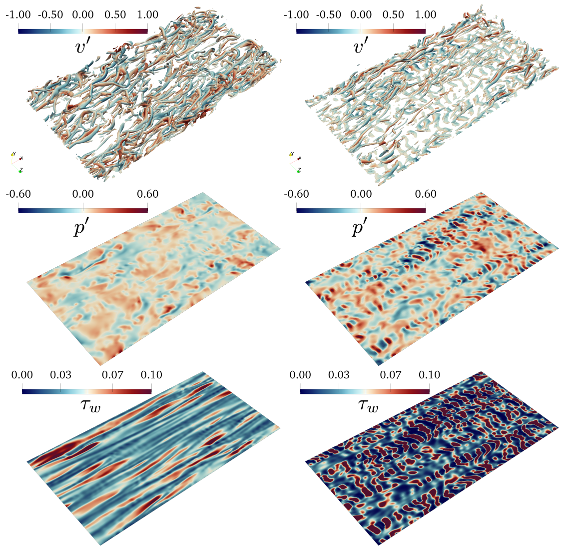

Figure 5. The comparison of near wall flow structures between $M_{3.5}R_{\text{inf}}$(left column) and $M_{3.5}R_{0.5}$(right column). Each column gives (from top to bottom) Q-criterion colored by wall normal velocity, pressure fluctuation on the wall and the wall shear stress.

Mean Flow Statistics Profiles of mean streamwise velocity with various lower wall permeability are shown in figure 7. All the values are normalized with the lower wall properties. The increase of mean wall shear causes the mean streamwise velocity to deviate from the baseline case. A decreasing acoustic resistance R, i.e., increasing wall permeability results in a larger deviation of the mean profile. The root-mean-square (RMS) wall normal velocity is plotted in figure 8. Due to the non-zero wall permeability, pressure fluctuations at the wall induce the non-zero wall normal velocity fluctuations, which explains the high value of RMS velocity right on the wall. As expected, higher permeability leads to stronger reaction on the wall and thus higher value of RMS wall velocity.

CONCLUSION

The supersonic turbulent channel flows over various wall acoustic permeability have been performed, with wall acoustic properties modeled by time domain impedance boundary conditions (TDIBC). A mass-spring-damper impedance model is adopted for TDIBC, whose resonating frequency is tuned to the characteristic frequency of energetic eddies. Simulation are performed for two bulk Mach numbers $M_b = 1.50, 3.50$ while keeping approximately the same viscous Reynolds number Re^*_τ. A wide range of acoustic resistance R has been examined. Significant changes in near wall turbulent structures have been observed for low enough acoustic resistance R, i.e., high

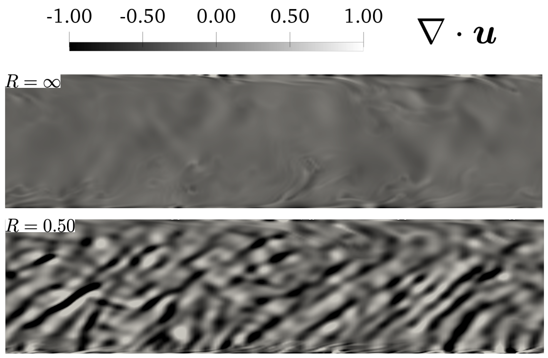

Figure 6. An $x - y$ plane contour plot of the dilation field for $M_b = 3.50$ with impermeable wall (top) and permeable wall (bottom with $R = 0.50$).

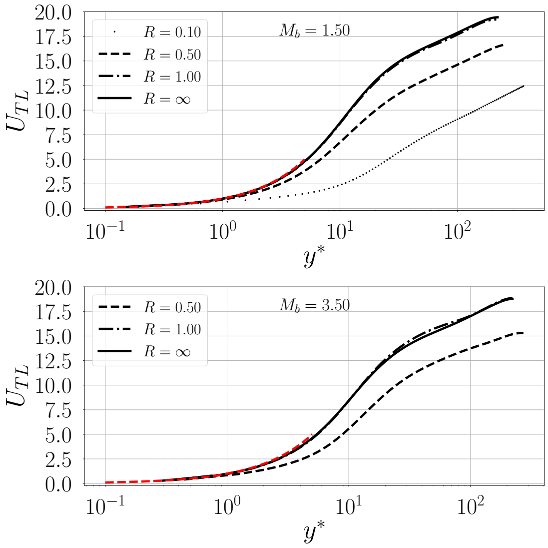

Figure 7. Mean streamwise velocity profile with various wall permeability for $M_b = 1.50$ (top) and $M_b = 3.50$ (bottom).

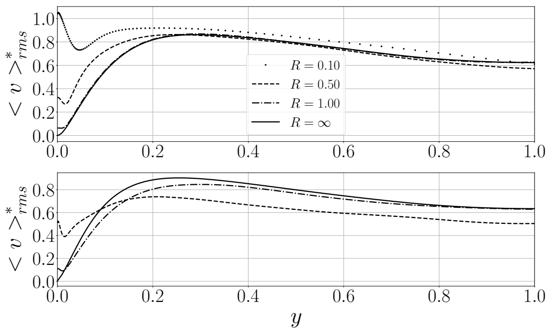

Figure 8. RMS wall normal velocity with various wall permeability for $M_b = 1.50$ (top) and $M_b = 3.50$ (bottom).

enough wall permeability. Spanwise rollers replace the typical seen streawise streaks and hairpin vortices near the wall, leaving a footprint of alternating pattern in pressure and wall shear stress. Rollers are found to strongly interact with the flow with sufficiently high wall permeability.

ACKNOWLEDGMENTS

The authors acknowledge the support of the Air Force Research Office of Scientific Research (AFOSR) 2018 Young Investigator Award (YIP) (FA9550-18-1-0292). Computational resources are provided by the Rosen Center for Advanced Computing (RCAC) at Purdue University and the Extreme Science and Engineering Discovery Environment (XSEDE).

APPENDIX

Auxiliary Differential Equations

Here the detailed derivations of ADE method are provided. The wall softness of n_0 oscillators that appears in (4) can be approximated by summation of rational functions:

$$\widehat{\widetilde{W}}(\omega) \approx \sum_{k=1}^{n_0} \left(\frac{\mu_k}{i\omega - p_k} + \frac{\mu_k^*}{i\omega - p_k^*} \right) \tag{9}$$

where the poles $p_k = c_k + id_k$ and residues $\mu_k = a_k + ib_k$. This form is sufficiently accurate for the three-parameter impedance model and no more complications are needed. Take the inverse Fourier transform of (9) and get

$$\begin{aligned}
\widetilde{W}(t) =& \sum_{k=1}^{n_0} \left(\mu_k e^{p_k t} + \mu_k^* e^{p_k^* t} \right) H(t) \\
=& \sum_{k=1}^{n_0} \left[(a_k + ib_k) e^{(c_k + id_k)t} + (a_k - ib_k) e^{(c_k - id_k)t} \right] H(t) \\
=& \sum_{k=1}^{n_0} \left[2a_k e^{c_k t} \cos(d_k t) - 2b_k e^{c_k t} \sin(d_k t) \right] H(t)
\end{aligned}$$

with this, the convolution in equation (4), denoted as $I = \int_0^t \widetilde{W}(\tau) v_n^{\text{out}}(t-\tau) d\tau$

$$\begin{aligned}
I =& \int_0^t \sum_{k=1}^{n_0} \left[2a_k e^{c_k \tau} \cos(d_k \tau) - 2b_k e^{c_k \tau} \sin(d_k \tau) \right] v_n^{\text{out}}(t-\tau) d\tau \\
=& \sum_{k=1}^{n_0} \int_0^t \left[2a_k e^{c_k \tau} \cos(d_k \tau) - 2b_k e^{c_k \tau} \sin(d_k \tau) \right] v_n^{\text{out}}(t-\tau) d\tau \\
=& \sum_{k=1}^{n_0} \int_0^t 2a_k e^{c_k (t-\tau)} \cos(d_k (t-\tau)) v_n^{\text{out}}(\tau) d\tau \\
& - \sum_{k=1}^{n_0} \int_0^t 2b_k e^{c_k (t-\tau)} \sin(d_k (t-\tau)) v_n^{\text{out}}(\tau) d\tau
\end{aligned}$$

Note that the last line utilizes the commutative property of convolution. Now define

$$\psi_k^{(1)}(t) = \int_0^t e^{c_k (t-\tau)} \cos(d_k (t-\tau)) v_n^{\text{out}}(\tau) d\tau \tag{10}$$

$$\psi_k^{(2)}(t) = \int_0^t e^{c_k (t-\tau)} \sin(d_k (t-\tau)) v_n^{\text{out}}(\tau) d\tau \tag{11}$$

taking derivatives of $\psi_k^{(1)}(t)$ and $\psi_k^{(2)}(t)$ with respect to time t we can obtain equation (5) and (6), then the domain-leaving wave can be obtained by

$$v_n^{\text{in}}(t) = -v_n^{\text{out}}(t) + \sum_{k=1}^{n_0} 2[a_k \psi_k^{(1)}(t) - b_k \psi_k^{(2)}] \tag{7}$$

And velocity or pressure fluctuation can be recovered from the relation

$$v'(t) = \left[v_n^{\mathrm{in}}(t) + v_n^{\mathrm{out}}(t)\right]/2 \tag{12}$$

$$p'(t) = \begin{cases} \left[v_n^{\mathrm{out}}(t) - v_n^{\mathrm{in}}(t)\right]/2, & \text{top boundary} \\ \left[v_n^{\mathrm{in}}(t) - v_n^{\mathrm{out}}(t)\right]/2, & \text{bottom boundary} \end{cases} \tag{13}$$

Application of TDIBC in Compressible Turbulent Channel Flows

To ensure the TDIBC is implemented correctly in the turbulent channel flow, wall normal velocity and pressure signals at the first grid point off the wall are taken to examine the cross spectrum contributions from each frequency. The magnitude and phase of the spectrum are plotted in figure 9. Good agreement is achieved in the low frequency range for both the magnitude and phase. The error gradually increases as frequency moves to higher values. Higher values of R has larger error at resonating frequency, which is probably due to the fact the signals are not taken on the wall.

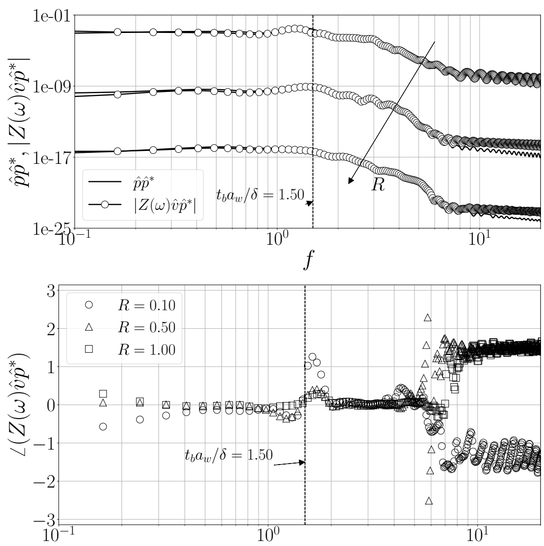

Figure 9. Magnitude (top and shifted) and phase (bottom) of cross-spectrum for $M_b = 1.50$ cases. The vertical dash line implies the resonating frequency that TDIBC is tuned to, where $t_b = \delta/U_b$.

REFERENCES

Allampalli, Vasanth, Hixon, Ray, Nallasamy, M & Sawyer, Scott D 2009 High-accuracy large-step explicit runge–kutta (hale-rk) schemes for computational aeroacoustics. *Journal of Computational Physics* **228** (10), 3837–3850.

Coleman, G.N., Kim, J. & Moser, R.D. 1995 A numerical study of turbulent supersonic isothermal-wall channel flow. *J. Fluid Mech.* **305**, 159–184.

Douasbin, Q, Scalo, C, Selle, L & Poinsot, T 2018 Delayed-time domain impedance boundary conditions (d-tdibc). *J. Comput. Phys.* **371**, 50–66.

Dragna, Didier, Pineau, Pierre & Blanc-Benon, Philippe 2015 A generalized recursive convolution method for time-domain propagation in porous media. *The Journal of the Acoustical Society of America* **138** (2), 1030–1042.

Fung, K. Y. & Ju, H. 2001 Broadband Time-Domain Impedance Models. *AIAA Journal* **39** (8), 1449–1454.

Fung, K-Y & Ju, Hongbin 2004 Time-domain impedance boundary conditions for computational acoustics and aeroacoustics. *Int. J. Comput. Fluid D.* **18** (6), 503–511.

Fung, K-Y, Ju, Hongbin & Tallapragada, BhanuPrakash 2000 Impedance and its time-domain extensions. *AIAA journal* **38** (1), 30–38.

Ingard, Uno 1959 Influence of fluid motion past a plane boundary on sound reflection, absorption, and transmission. *The Journal of the Acoustical Society of America* **31** (7), 1035–1036.

Jiménez, J., Uhlmann, M., Pinelli, A. & Kawahara, G. 2001 Turbulent shear flow over active and passive porous surfaces. *J. Fluid Mech.* **442**, 89–117.

Kinsler, Lawrence E, Frey, Austin R, Coppens, Alan B & Sanders, James V 1999 Fundamentals of acoustics. *Fundamentals of Acoustics, 4th Edition, by Lawrence E. Kinsler, Austin R. Frey, Alan B. Coppens, James V. Sanders, pp. 560. ISBN 0-471-84789-5. Wiley-VCH, December 1999.* p. 560.

Moser, Robert D., Kim, John & Mansour, Nagi N. 1999 Direct numerical simulation of turbulent channel flow up to Re = 590. *Phys. Fluids* **11** (4), 943–945.

Myers, MK 1980 On the acoustic boundary condition in the presence of flow. *J. Sound Vib.* **71** (3), 429–434.

Nagarajan, S., Lele, S.K. & Ferziger, J.H. 2003 A robust high-order compact method for large eddy simulation. *J. Comput. Phys.* **191**, 392–419.

Özyörük, Y. & Long, L. N. 1997 A time-domain implementation of surface acoustic impedance condition with and without flow. *J. Comput. Acou.* **5** (3), 277 – 296.

Rienstra, S. W. 2006 Impedance Models in Time Domain, including the Extended Helmholtz Resonator Model. In *12th AIAA/CEAS Aeroacoustics Conference*.

Scalo, Carlo, Bodart, Julien & Lele, Sanjiva K. 2015 Compressible turbulent channel flow with impedance boundary conditions. *Phys. Fluids* **27** (035107).

Tam, C. K. W. & Auriault, L. 1996 Time-domain Impedance Boundary Conditions for Computational Aeroacoustics. *AIAA Journal* **34** (5), 917 – 923.

Trettel, A. & Larsson, J. 2016 Mean velocity scaling for compressible wall turbulence with heat transfer. *Phys. Fluids* **28**, 026102.

Troian, Renata, Dragna, Didier, Bailly, Christophe & Galland, Marie-Annick 2017 Broadband liner impedance eduction for multimodal acoustic propagation in the presence of a mean flow. *Journal of Sound and Vibration* **392**, 200–216.

Ulerich, Rhys David *et al.* 2014 Reducing turbulence- and transition-driven uncertainty in aerothermodynamic heating predictions for blunt-bodied reentry vehicles. PhD thesis.

Vreman, A. W. 2004 An eddy-viscosity subgrid-scale model for turbulent shear flow: Algebraic theory and applications. *Phys. Fluids* **16** (10), 3670.